GaitTracker: 3D Skeletal Tracking for Gait Analysis Based on Inertial Measurement Units

LEI XIE, PEICHENG YANG, and CHUYU WANG, State Key Laboratory for Novel Software Technology, Nanjing University, China
TAO GU, School of Computing, Macquarie University, Australia
GAOLEI DUAN, XINRAN LU, and SANGLU LU, State Key Laboratory for Novel Software Technology, Nanjing University, China

Gait rehabilitation is a common method of postoperative recovery after the user sustains an injury or disability. However, traditional gait rehabilitations are usually performed under the supervision of rehabilitation specialists, which implies that the patients cannot receive adequate gait assessment anytime and anywhere. In this article, we propose GaitTracker, a novel system to remotely and continuously perform gait monitoring and analysis by three-dimensional (3D) skeletal tracking in a wearable approach. Specifically, this system consists of four Inertial Measurement Units (IMU), which are attached on the shanks and thighs of the human body. According to the measurements from these IMUs, we can obtain the motion signals of lower limbs during gait rehabilitation. By adaptively synchronizing coordinate systems of different IMUs and building the geometric model of lower limbs, the exact gait movements can be reconstructed, and gait parameters can be extracted without any prior knowledge. GaitTracker offers three key features: (1) *a unified 3D skeletal model* to depict the precise gait movement and parameters in 3D space, (2) *a coordinate system synchronization scheme* to perform space synchronization over all the IMU sensors, and (3) *an automatic estimation method* for the user-specific geometric parameters. In this way, GaitTracker is able to accurately perform 3D skeletal tracking of lower limbs for gait analysis, such as evaluating the gait symmetry and the gait parameters including the swing/stance time. We implemented GaitTracker and evaluated its performance in real applications. The experimental results show that, the average error for skeleton angle estimation, joint displacement estimation, and gait parameter estimation are 3°, 2.3%, and 3%, respectively, outperforming the state of the art.

CCS Concepts: • **Human-centered computing → Ubiquitous and mobile computing;**

Additional Key Words and Phrases: 3D skeletal tracking, inertial sensing, wearable devices, gait analysis

This work is supported in part by National Natural Science Foundation of China under Grant Nos. 61832008, 61872174, 61902175, and 61802169; the Key R&D Program of Jiangsu Province under Grant No. BE2020001-3; JiangSu Natural Science Foundation under Grants No. BK20190293 and BK20180325; Australian Research Council (ARC) Discovery Project grant DP190101888. This work is partially supported by Collaborative Innovation Center of Novel Software Technology and Industrialization.

Authors' addresses: L. Xie (corresponding author), P. Yang, C. Wang (corresponding author), G. Duan, X. Lu, and S. Lu, State Key Laboratory for Novel Software Technology, Nanjing University, China; emails: lxie@nju.edu.cn, 18362903155@163.com, chuyu@nju.edu.cn, cakelnju@qq.com, luxinran@smail.nju.edu.cn, sanglu@nju.edu.cn; T. Gu, School of Computing, Macquarie University, Australia; email: tao.gu@mq.edu.au.

1550-4859/2022/03-ART27 $15.00
https://doi.org/10.1145/3502722

ACM Reference format:
Lei Xie, Peicheng Yang, Chuyu Wang, Tao Gu, Gaolei Duan, Xinran Lu, and Sanglu Lu. 2022. GaitTracker: 3D Skeletal Tracking for Gait Analysis Based on Inertial Measurement Units. *ACM Trans. Sen. Netw.* 18, 2, Article 27 (March 2022), 27 pages.
https://doi.org/10.1145/3502722

1 INTRODUCTION

1.1 Motivation

Gait rehabilitation is commonly used for postoperative recovery to assist patients in evaluating and recovering their ability of walking after sustaining an injury or disability. The potential applications may include **six-minute walking test (6MWT)** [18] and *postoperative recovery evaluation* [7, 9]. Specifically, the 6MWT is an exercise test to measure the functional status of patients with moderate and severe heart and lung diseases. For example, the patients after the intensive care in ICU are usually required to perform 6MWT and accurately evaluate the total walking distance, step length, step speed, and so on. Moreover, the *postoperative recovery evaluation* requires gait analysis of the patients after surgery, including the stride/step length, cycle/swing/stance time, symmetry, and so on. Traditionally, gait rehabilitation is performed under the supervision of rehabilitation specialists, because inappropriate and incorrect actions may cause secondary injury. However, in reality, patients may not be able to receive adequate gait rehabilitation services due to a lack of rehabilitation specialists. Monitoring and analyzing gaits automatically and remotely has been a great demand in recent years. In such a paradigm, an intelligent sensing system is typically deployed to reconstruct gait movements so that patients will be able to access rehabilitation services anytime and anywhere, and gait assessment can be done remotely by rehabilitation specialists.

1.2 Limitation of Prior Art

Existing approaches to gait monitoring fall into three categories, i.e., computer vision based, wireless signal based, and wearable sensor based. The computer vision-based approaches [6, 8, 11, 16] have been proposed since the late 2000s to monitor and capture the gait movements of patients directly using cameras. However, the use of cameras has several limitations. A camera typically has a limited angle of view and may be vulnerable to occlusion and poor lighting in indoor environments. In addition, real-time monitoring will generate a large volume of video streaming data that may consume much network bandwidth when uploaded to the server for analysis. Moreover, the use of camera may violate user privacy, and so far there are no reliable solutions available. Wireless signals such as WiFi [10, 24, 26], **Ultra Wide-Band (UWB)** [3], RFID [22], and mmWave [15, 28] have been exploited to monitor the gait movements of a patient. These approaches offer a device-free and lightweight solution. However, wireless signals are susceptible to indoor multipath effects, and thus these approaches may be easily affected by other human subjects in the environment. Wearable sensors have also been widely used in gait monitoring. These approaches require attaching wearable sensors, e.g., pressure sensors [14] and **Inertial Measurement Units (IMU)** sensors [4, 13, 19, 30], to the limbs of human body for capturing gait movements. Among these sensors, IMU sensors become increasingly popular nowadays due to their low cost and high reliability. Note that the attached IMU can only reflect the movement of the bounded limb [21, 23, 25, 29]. Since the leg is not a rigid structure, i.e., the movement of the thigh is not identical to the shank, multiple IMU sensors are required to depict the complete posture of the entire leg. IMU sensors have been attached to the thighs and shanks of a human subject to monitor gait movements in Reference [4]. This system uses an inverse pendulum model to estimate gait parameters. However, the coordinate systems of different IMU sensors are not synchronized, and their model requires

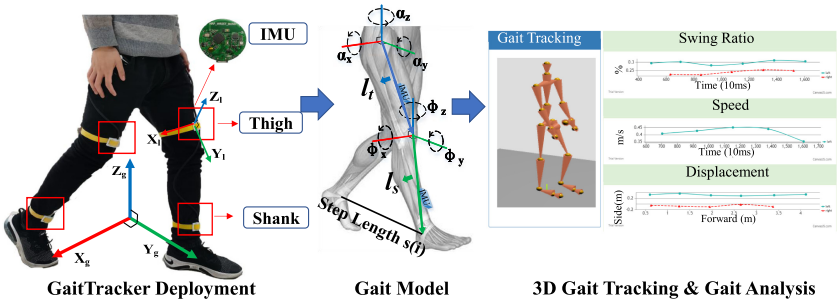

Fig. 1. GaitTracker System: four IMUs are attached on the shanks and thighs of the human body, according to the IMU measurements and the geometric model of the gait, the exact gait movements can be reconstructed in 3D space and the gait parameters can be extracted without any prior knowledge.

prior knowledge of the lower limb length of a subject. Synchronizing multiple sensors can be done using magnetometer, as demonstrated in Reference [32]. In this way, sensor data collected from different limbs can be integrated to build a unified 3D gait model. However, indoor magnetic field may vary from time to time and be susceptible to the surrounding environment. To avoid requiring the prior knowledge of user-specific parameters, Mannini et al. mount inertial sensors on the foot to calculate spatial parameters based on machine learning models [13], but they need to collect enough training data to estimate the user-specific parameters.

1.3 Technical Challenges

In light of the limitations of existing wearable sensor-based approaches, we aim to address the following two challenges for effective gait monitoring and analysis.

The first challenge is to adaptively synchronize coordinate systems of different IMUs to perform the multi-sensor fusion. Since the measurements of IMUs are based on the local coordinate system of each device, which keeps changing all the time, it is essential to synchronize the coordinate systems of different IMUs in the spatial dimension, such that the IMU measurements can be depicted in a consistent manner for gait monitoring. To tackle this challenge, we first design an adaptive complementary filtering algorithm to combine the accelerator and gyroscope measurements during a specified time window so as to avoid high-frequency jitters and drift errors caused by sensor defects. Then, according to the data fluctuation characteristics of acceleration and angular velocity during the process of walking forward, we use the **Principal Component Analysis (PCA)** to extract a consistent forward direction from linear acceleration as the longitudinal axis and extract a consistent lateral direction from angular velocity as the lateral axis. In this way, by referring to the consistent forward/lateral direction and the gravity direction, we are able to achieve coordinate system synchronization for different IMU sensors.

The second challenge is to build the user-specific geometric model of lower limbs without requiring any prior knowledge in advance, i.e., the limb length. Most of the existing work tracks gait movements based on the exact length of user's lower limbs and requires the user to manually specify this parameter or provide enough training data to estimate the parameter in advance. This is neither convenient nor practical for realistic applications. Besides, we realize that it does not work to estimate the limb length by simply positioning the adjacent thigh/shank sensors, because the position estimated by the quadratic integration of acceleration leads to non-negligible errors accumulated with time. To tackle this challenge, we investigate the geometric model of human body and propose a regression model to derive the shank and thigh length according to the relationship between the stride length and rotation angle/length of lower limbs. This solution does not require

prior knowledge about the user's lower limbs. Based on that, we can further compute the gait parameters without any prior knowledge.

1.4 Our System

In this article, we propose GaitTracker, an IMU-based three-dimensional (3D) skeletal tracking system for gait monitoring and analysis. GaitTracker aims to achieve both 3D gait motion tracking and gait parameter estimation, which facilitate rehabilitation specialists with complete gait analysis and assessment for patients. The system offers three key features: (1) *a unified 3D skeletal model* to depict the precise gait movement and parameters in 3D space, (2) *a coordinate system synchronization scheme* to perform space synchronization over all the IMU sensors, and (3) *an automatic estimation method* for the user-specific geometric parameters. In GaitTracker, IMU sensors are attached to the thighs and shanks of a subject to collect motion data. By measuring the acceleration and angular velocity of the corresponding locations from these IMUs, we can obtain the motion signals of the lower limbs during gait rehabilitation. By adaptively synchronizing coordinate systems of different IMUs and building the geometric model of lower limbs, the exact gait movements can be reconstructed and gait parameters can be extracted without any prior knowledge. Therefore, GaitTracker is able to accurately perform *3D skeletal tracking* of lower limbs for gait analysis, such as evaluating the gait symmetry and the gait parameters including the swing/stance time. Figure 1 gives an overview of the model, deployment, and data analysis of GaitTracker. Compared with the work done in Reference [32] that uses magnetometers to synchronize the coordinates of different IMU sensors, we use accelerators and apply PCA to align these coordinates, eliminating the problem of unstable magnetic field in the indoor environments. In addition, different from the existing approaches [13, 19] that calculate gait parameters based on the prior knowledge of limb length, empirical coefficients or the large training data, GaitTracker can directly estimate the gait parameters as well as the limb length based on the multiple inertial sensors without any prior information.

1.5 Contributions

In this article, we make three main contributions as follows. (1) To synchronize the coordinates of different IMUs without magnetometer, we introduce PCA to determine the unique global coordinate system. Specifically, we utilize PCA to derive the longitudinal axis from linear acceleration and lateral axis from angular velocity. Based on these two axes, we can derive a global coordinate system that is consistent among all IMU sensors. (2) To estimate the spatial parameters of gait such as the limb length, we use a regression model to derive the shank/thigh length of users by exploiting the relationship in the geometric model of human body. This does not require any prior knowledge from the user in advance. (3) We implemented a prototype system of GaitTracker[1] and evaluated its performance in the real environment. Our experimental results show that the average error of skeleton angle estimation is 3°, the average error of joint displacement estimation is 0.23 m for every 10 m, and the average error of gait parameter estimation is 3%, outperforming the state of the art [4, 13, 19, 30].

2 RELATED WORK

Computer Vision-based Approach leverages the camera to capture gait movements. Moataz et al. [6] utilize the depth camera Kinect to obtain the joint positions in the global coordinate system and then estimate the gait parameters from these joint positions. Kuhman et al. [11] use a multiple-camera system and multiple reflective markers to measure the translations and rotations

[1]A demo of GaitTracker can be downloaded in the following web link: https://cs.nju.edu.cn/lxie/demo/gaittracker.mp4.

of lower limbs. Gu et al. [8] propose a 3D reconstruction algorithm to estimate the joint positions on the legs based on the images from a single RGB camera and then calculate the gait parameters. However, camera has limited angle of view and can be easily affected by indoor occlusion and poor lighting. Moreover, transferring raw video streaming data to the server can consume large bandwidth, and the critical gait parameters cannot be efficiently extracted until the whole video is uploaded.

Wireless Signal-based Approach uses wireless signals and leverages signal variations during walking to estimate the gait parameters [3, 10, 15, 22, 24, 26–28, 31]. Wang et al. [26] utilize the variations of WiFi signals reflected by a walking human subject to estimate the temporal gait parameters. Anderson et al. [3] design a foot-mounted UWB sensor and deploy two UWB sensors on each foot to estimate the stride length from UWB signals. Wang et al. [22] attach RFID tags to the limbs of a subject for tracking body movements and estimating the limb rotations through the extracted phase features. Xue et al. [28] are the first to construct the 3D human mesh using the mmWave signals that bounce off the human body; they encode a 3D human model by analyzing the 3D point cloud generated from the mmWave signals based on a deep learning framework. Zhao et al. [31] design a convolutional neural network architecture to infer 3D human skeletons from RF signals. Jiang et al. [10] utilize WiFi signals to reconstruct 3D skeletons composed of the joints on both limbs and torso of the human body based on a deep learning model. However, wireless signals may be susceptible to multipath effect and easily affected by other moving subjects in the environment.

Wearable Sensor-based Approach uses multiple motion sensors [4, 13, 19, 30] attached to lower limbs or pressure sensors [14] for measuring motion signals. Note that the IMU usually only reflects the movement of the bounded limb [20, 21, 23, 29]. Since the leg is not a rigid structure, i.e., the movement of the thigh is not identical to the shank, it is difficult to use only a single IMU to construct the entire leg posture. Shen et al. [21] creatively propose a motion model to track the arm posture with only one smartwatch. They further design a particle filter-based technique to improve the arm motion tracking by jointly estimating the location and orientation of smartwatch [20]. However, both the two works rely on the assumption that the torso is static and the shoulder position is fixed. While for the gait monitoring, the whole body actually moves in the 3D space during the walking process. Therefore, multiple IMU sensors are required to track the leg motion. Bennett et al. [4] attach inertial sensors on the thighs and shanks to monitor gait movements. They use the **Extended Kalman Filter (EKF)** to model human leg as a two-link revolute robot. The model and the inertial measurements are used to estimate the human gait parameters and walking distance. However, the coordinate systems for different IMU sensors are not synchronized. Thus, high-frequency jitters and drift errors caused by sensor defects could affect the robustness of the system. Moreover, the EKF model requires subjects to manually provide their user-specific geometric parameters of lower limbs as prior knowledge. To avoid requiring the prior knowledge of user-specific geometric parameters, **Inertial Navigation System (INS)** [30] proposes an inequality-constrained Zero-Velocity-Updates–aided INS algorithm to automatically estimate the gait parameters. However, different coordinate systems of IMU sensors on the feet are still not synchronized in this system. Mannini et al. [13] and Sant'Anna et al. [19] mount inertial sensors on shoes to capture the movement of each step. Mannini et al. [13] calculate the spatial gait parameters from a machine learning model based on large training data. Sant'Anna et al. [19] develop a system to deal with several gait abnormalities and evaluate quantitative gait analysis with both in-lab and *in situ* evaluations. However, the above two approaches perform gait analysis without constructing any unified 3D model and coordinate synchronization, and the user-specific prior knowledge is required.

Table 1. GairTracker vs. Wearable Sensor-based Approach

	3D Model of Lower Limbs	Coordinate Synchronization	Need Prior knowledge
GaitTracker	Yes	Yes	No
EKF [4]	Yes	No	Yes
INS [30]	No	No	No
Sant'Anna et al. [19]	No	No	Yes
Mannini et al. [13]	No	No	Yes

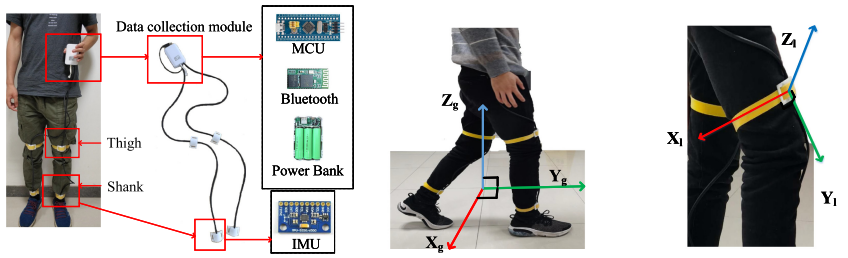

(a) Gait Tracker & Deployment (b) Global Coordinate System (c) Local Coordinate System

Fig. 2. The deployment of GaitTracker.

In this article, GaitTracker aims to perform gait monitoring and analysis by tracking the 3D skeleton of a subject with inertial sensors. Different from the existing approaches, by performing *coordinate system synchronization*, GaitTracker builds a unified *3D skeletal model* for lower limbs to accurately track the precise gait in 3D. Moreover, GaitTracker does not require any *user-specific prior knowledge*, offering both convenience and adaptivity to users. A comparison with other wearable approaches is given in Table 1.

3 EMPIRICAL STUDY

To investigate the gait parameters from motion data, we first conduct several experiments based on our system, GaitTracker. As shown in Figure 2(a), GaitTracker consists of four IMUs and a data collection module powered by a power bank. Each IMU has an accelerometer, measuring both the earth's gravitational acceleration and linear acceleration, and a gyroscope, measuring angular velocity. The data collection module collects sensor data from the IMUs via the cable or Bluetooth. During our experiments, we attach four IMUs to the lower limbs of a subject, i.e., two IMUs are placed on the ankles and the other twos are placed on the knees, for collecting both acceleration and angular velocity as motion data. For ground truth, we deploy OptiTrack [1], a precise motion capture and 3D tracking system, to capture the positions and orientations of the IMUs. For each IMU, we attach three reflective markers of OptiTrack on the surface of IMU, which are used to estimate the corresponding positions and orientations.

In GaitTracker, we define the global coordinate system as shown in Figure 2(b), where the initial facing orientation of the subject is the Y_g axis, the opposite direction of the gravity is the Z_g axis, and the direction to the right relative to the body is the X_g axis. Each IMU has a local coordinate system as shown in Figure 2(c), where the X_l axis is to the right of IMU's surface, the Z_l axis is perpendicular to IMU's surface, and the Y_l axis is to the up of IMU's surface. Since OptiTrack captures the orientations of IMUs relative to the global coordinate system, we convert the motion data from the local coordinate system to the global coordinate system. Specifically, we use a 3×3 rotation matrix $\mathbf{R_{lg}(t)}$ measured from OptiTrack to project IMU's measurements to the global coordinate. We can then extract the linear acceleration $\mathbf{a_g(t)}$ and angular velocity $\mathbf{w_g(t)}$ in the

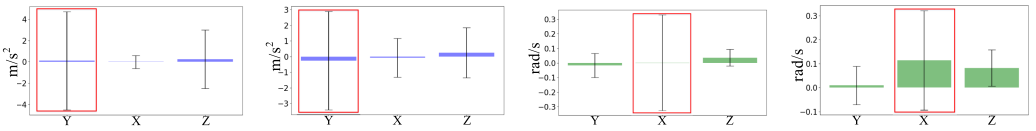

(a) Acceleration of Shank (b) Acceleration of Thigh (c) Gyroscope of Shank (d) Gyroscope of Thigh

Fig. 3. The mean and standard deviation of motion data in different axes.

global coordinate from accelerometer $\mathbf{a_l(t)}$ and gyroscope measurements $\mathbf{w_l(t)}$, respectively, as follows:

$$\begin{cases} \mathbf{a_g(t)} = \mathbf{R_{lg}(t)} \cdot \mathbf{a_l(t)}, \\ \mathbf{w_g(t)} = \mathbf{R_{lg}(t)} \cdot \mathbf{w_l(t)}. \end{cases} \tag{1}$$

We further use the extracted motion parameters $\mathbf{a_g(t)}$ and $\mathbf{w_g(t)}$ to investigate the gait features.

3.1 Observation 1

As the human subject is walking along a straight line in the Y_g axis, the fluctuation of acceleration is concentrated on the forward direction, i.e., Y_g, and the fluctuation of angular velocity is concentrated on the lateral direction, i.e., X_g in the global coordinate system.

We let the subject wear GaitTracker and walk along the Y_g axis for 20 s. Meanwhile, we measure motion data and then convert to the global coordinate system according to the rotation matrix of OptiTrack. Figure 3 shows the mean and standard deviation of linear acceleration and angular velocity in different axes of the global coordinate. We observe that the linear acceleration variance of thighs and shanks in the Y_g axis is significantly larger than that in other axes, and the angular velocity variance of shanks and thighs in the X_g axis is significantly larger than that in other axes. This implies that when the human subject walks in the straight line, the acceleration of shanks and thighs fluctuates mainly in the walking direction, and the angular velocity fluctuates mainly in the lateral direction of human body.

3.2 Observation 2

The length of lower limbs is an essential factor for estimating the spatial gait parameters, e.g., step length and step width. It can be estimated based on the stride length and the rotation angles of lower limbs.

The *Stride length*, *step length*, *step width*, and *knee joint angles* are common and important spatial parameters in gait analysis. Furthermore, the temporal parameters in gait analysis such as *cycle time*, *swing time*, as well as *stance time* are further used together with the spatial parameters to analyze the gait movements and generate more complex parameters, e.g., the *symmetry* of the gaits. In addition to these gait parameters, the user-specific parameters, e.g., the length of lower limbs (including the shank length and thigh length), are important parameters to calculate the gait parameters, especially the spatial parameters. As shown in Figure 4(a), thigh length is the distance between hip and knee as l_t, and shank length is the distance between knee and ankle as l_s.

We find that the length of lower limbs can be estimated from the measurements of the *stride length*. *Stride length* is a common gait parameter that can be used to measure the symmetry characteristics of gait rehabilitation. It can be calculated using the following methods. The first method is to directly measure the distance between successive ground contacts of the same foot. As shown in Figure 4(a), $\mathbf{p(i)}$ and $\mathbf{p(i+1)}$ are successive ground contacts of the left foot. The *stride length* is equal to the distance between $\mathbf{p(i)}$ and $\mathbf{p(i+1)}$, i.e., $d(i)$, which can be calculated based on motion data collected from the IMU attached to the specific foot. The second method is to calculate the *stride length* by summing up two successive step lengths. As shown in Figure 4(a), the *stride length* is equal to the sum of two adjacent *step lengths*, i.e., $s(i)$ and $s(i+1)$, when the human subject takes

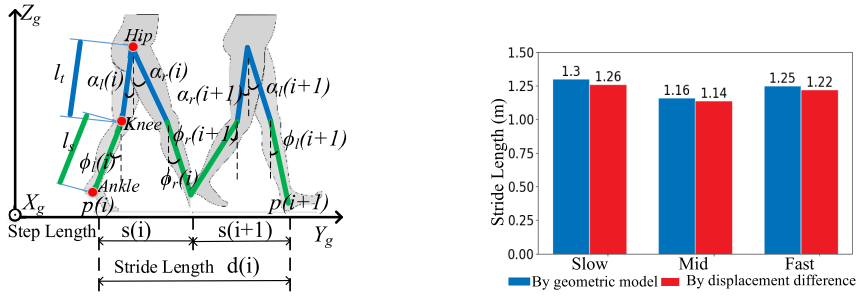

(a) The Geographic Model (b) Estimate the Stride Length

Fig. 4. The relationship between the length of lower limbs and stride length.

two continuous steps. For each *step length* $s(i)$ or $s(i+1)$, we use the geometric model [22] to calculate the *step length* according to the length and rotation angles of shanks and thighs. Therefore, we can manually measure the length of lower limbs and calculate the rotation angles from the IMU measurements, then further use these parameters to calculate the *stride length*.

We conduct experiments by asking the subject to walk at different speeds v, i.e., slow ($v \leq 1$ m/s), mid(1m/s $\leq v \leq$ 2 m/s), and fast speed ($v \geq 2$ m/s), and evaluate the two methods by comparing the similarity between *stride lengths*. As shown in Figure 4(b), we find that the results of these two methods are consistent. Based on our observations, by combining the two measurements of stride length, given the *stride length* d as well as the rotation angles of thighs α and shanks ϕ, we can deduce the length of thighs l_t and shanks l_s, respectively. In this way, we can further figure out the spatial gait parameters, e.g., step length and step width. We will introduce the detailed solution in Section 4.2.

3.3 Summary

We now summarize the key findings as follows based on the above empirical study. (1) For each IMU, the forward and lateral directions of walking are the major fluctuation directions of linear acceleration and angular velocity, respectively. Therefore, we can estimate X_g and Y_g by calculating the major fluctuation directions of motion data. This provides a chance to align local coordinate systems of all the IMUs to the common global coordinate system. (2) The length of lower limbs, which is essential for the gait parameters, can be estimated from the measurements of the stride length and the rotation angles of the joints on lower limbs. Specifically, the length of lower limbs can be inferred from stride length and rotation angles of shanks and thighs without any prior knowledge. Based on the length of lower limbs, we can further calculate the spatial gait parameters.

4 MODELING

4.1 Coordinate System Transformation

As shown in Figure 2(c), each IMU contructs its **Local Coordinate System (LCS)** and collects its motion data. However, when the subject walks, the LCSs will be changed continuously. It is essential to synchronize the coordinate systems of different IMUs in the spatial dimension so that IMU measurements can be depicted in a consistent manner for gait monitoring. Instead of directly using the Earth's coordinate system (i.e., magnetometer), which is unreliable in the indoor environments, we build a global coordinate system based on the moving direction of the human subject, as shown in Figure 2(b). To perform the coordinate system transformation, we first define a **Reference Coordinate System (RCS)** for each IMU at the initial time t_0. For each IMU, we transform its local coordinate system at time t to the reference coordinate system at time t_0. Then, we

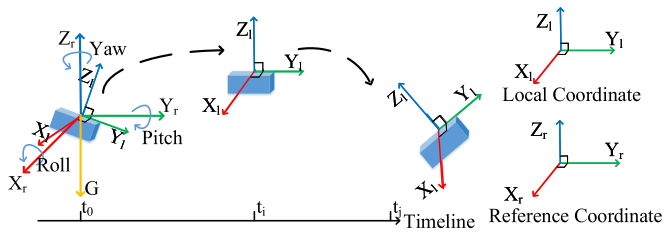

Fig. 5. Local coordinate vs. reference coordinate during walking.

transform different reference coordinate systems to the **Global Coordinate System (GCS)**, which can be deduced according to the data fluctuation characteristics of acceleration and angular velocity.

4.1.1 Local Coordinate System to Reference Coordinate System. For each IMU, its LCS keeps changing as it moves along with the human subject. Therefore, we need to choose a RCS, which is relatively stable to the earth coordinate system, and then transform the dynamic LCS to the stable RCS. We define RCS for each IMU as shown in Figure 5, which is determined at the initial time t_0 when the system starts. For the RCS, the Z_r axis is opposite to the direction of gravity, X_r axis is the projection of X_l axis in LCS at the initial time t_0 on the ground plane and Y_r axis is defined as the vector product $Z_r \times X_r$. Then, for the consecutive time t, we use the quaternion $\mathbf{q_{lr}(t)}$ to transfer LCS to RCS.

At the initial time t_0, because the accelerometer only measures the gravitational acceleration when the IMU is stationary, we can identify the initial $\mathbf{q_{lr}(t_0)}$ from the accelerometer measurements for the coordinate system transformation. Assuming that the acceleration at t_0 is $\mathbf{a_l(t_0)}$, we can calculate the initial Euler angles with roll $\varphi = \arctan \frac{a_{l,y}(t_0)}{a_{l,z}(t_0)}$, pitch $\theta = \arctan \frac{-a_{l,x}(t_0)}{\sqrt{a_{l,y}(t_0)^2 + a_{l,z}(t_0)^2}}$ and yaw $\psi = 0$. Then, the transformation quaternion $\mathbf{q_lr(t_0)}$ can be inferred from these Euler angles [5] as

$$\mathbf{q_{lr}(t_0)} = \begin{bmatrix} \cos\frac{\varphi}{2}\cos\frac{\theta}{2}\cos\frac{\psi}{2} + \sin\frac{\varphi}{2}\sin\frac{\theta}{2}\sin\frac{\psi}{2} \\ \sin\frac{\varphi}{2}\cos\frac{\theta}{2}\cos\frac{\psi}{2} - \cos\frac{\varphi}{2}\sin\frac{\theta}{2}\sin\frac{\psi}{2} \\ \cos\frac{\varphi}{2}\sin\frac{\theta}{2}\cos\frac{\psi}{2} + \sin\frac{\varphi}{2}\cos\frac{\theta}{2}\sin\frac{\psi}{2} \\ \cos\frac{\varphi}{2}\cos\frac{\theta}{2}\sin\frac{\psi}{2} - \sin\frac{\varphi}{2}\sin\frac{\theta}{2}\cos\frac{\psi}{2} \end{bmatrix}. \tag{2}$$

In the consecutive time t, $\mathbf{q_{lr}(t)}$ can be updated by either the angular velocity or the accelerated velocity. For the angular velocity, we can calculate the updated quaternion $\mathbf{q^w_{lr}(t)}$ as

$$\begin{cases} \mathbf{q^w_{lr}(t)} = \mathbf{q_{lr}(t-1)} + \delta_{\mathbf{q_{lr}}}\mathbf{(t)}\triangle t, \\ \delta_{\mathbf{q_{lr}}}\mathbf{(t)} = \frac{1}{2}\mathbf{q_{lr}(t-1)} \otimes \mathbf{w_l(t)}. \end{cases} \tag{3}$$

Here $\mathbf{w_l(t)}$ is the gyroscope measurement at time t and $\triangle t$ is the sampling interval. For the accelerated velocity, the updated quaternion $\mathbf{q^a_{lr}(t)}$ can be estimated by the accelerometer measurements with the gradient descent algorithm [12].

Even though we can estimate the quaternion from the acceleration or the angular velocity, the updated quaternion $\mathbf{q^w_{lr}(t)}$ exists a slow drift, and the updated quaternion $\mathbf{q^a_{lr}(t)}$ suffers from significant jitters around the high-frequency band. To solve the problem, we design an *adaptive complementary filter* [12] to combine the two quaternions. Assuming that the divergence rate of $\mathbf{q^w_{lr}(t)}$ is β_w and the convergence rate of $\mathbf{q^a_{lr}(t)}$ is β_a, the weighted β_w is equal to the weighted β_a when the IMU is moving. Since $\mathbf{q^a_{lr}(t)}$ is more credible when IMU is stationary, we give $\mathbf{q^a_{lr}(t)}$ a higher

weight when IMU moves slowly. Therefore, the complementary filter can be expressed as

$$\begin{cases} \mathbf{q_{lr}(t)} = \gamma(t) \cdot \mathbf{q^a_{lr}(t)} + (1-\gamma(t))\mathbf{q^w_{lr}(t)}, \\ \gamma(t) = \frac{\beta_a \cdot \eta(t)}{\beta_w + \beta_a \cdot \eta(t)}. \end{cases} \tag{4}$$

Here $\eta(t)$ is used to adjust the weight of $\mathbf{q^a_{lr}(t)}$. It guarantees that $\mathbf{q_{lr}(t)}$ is calibrated when IMU is stationary, and it is expressed as

$$\eta(t) = \begin{cases} e^{k(\frac{c-\|\mathbf{w_l(t)}\|}{c})} & \text{when } \|\mathbf{w_l(t)}\| < c \\ 1 & \text{when } \|\mathbf{w_l(t)}\| \geq c \end{cases}. \tag{5}$$

Here $\|\mathbf{w_l(t)}\|$ is the magnitude of the angular velocity, c is the threshold to determine whether the sensor is moving, and k is the experiential parameter. In our system, we set c to 0.1 and set k to 2.5, empirically.

4.1.2 Reference Coordinate System to Global Coordinate System. Since different IMUs of GaitTracker may have different initial attitudes, their RCSs at time t_0 are different from each other. Thus, we need to align all the RCSs to a consistent GCS. According to the observation in Section 3.1, *all the IMUs attached on the lower limbs share a consistent forward direction and lateral direction when the human subject walks forward.* Therefore, we define GCS according to the initial moving direction of the human subject as shown in Figure 2(b) and then align the RCSs of all the IMUs to the unique GCS. Specifically, the Z_g axis in the GCS is consistent with the Z_r axis in the RCS, the Y_g axis in the GCS is consistent with the forward direction, and the X_g axis is consistent with the lateral direction on the horizontal plane. Therefore, the difference between RCS and GCS can be expressed by the rotation angle θ between the Y_g and Y_r (or X_g and X_r) axis in the horizontal plane.

Since GCS and RCS share the same Z axis, we propose to determine GCS based on two methods: (1) the *acceleration-based method* (calculating the Y_g axis from the forward direction) and (2) the *angular velocity-based method* (calculating the X_g axis from the lateral direction). For the first method to figure out the Y_g axis, since the fluctuation of acceleration is concentrated on the Y_g axis, we use PCA to extract the principal component in acceleration and regard the direction as Y_g. Because X_g and Y_g are on the consistent horizontal plane, X_g can be inferred from $Y_g \times Z_g$, which simply rotates Y_g 90° counterclockwise around Z_g. Finally, we can deduce the rotation angle based on the acceleration measurements as shown in Figure 6, which is denoted as θ_a. For the second method to figure out X_g axis, we can similarly use PCA to extract the principal component based on the angular velocity and regard the direction as X_g. Then, we can extract the rotation angle θ_w from angular velocity.

Due to the inevitable measurement error of the two estimations, we further combine the two rotation angle estimations as a *hybrid method*. We use a weighted average of the two estimations to obtain the optimal results. Specifically, when we use PCA to calculate the principal fluctuation component, we can obtain its *explained variance*. The larger *explained variance* means that the fluctuation of corresponding component is more obvious. Therefore, the optimal rotation angle $\widehat{\theta}$ can be calculated by fusing θ_a and θ_w as follows:

$$\widehat{\theta} = \frac{v_a}{v_a + v_w}\theta_a + \frac{v_w}{v_a + v_w}\theta_w, \tag{6}$$

where v_a and v_w are corresponding explained variances. $\widehat{\theta}$ indicates the rotation angle between the $\hat{x}$ and X_R as shown in Figure 6. Thus, the rotation matrix $\mathbf{R_{rg}}$ between RCS and GCS of each

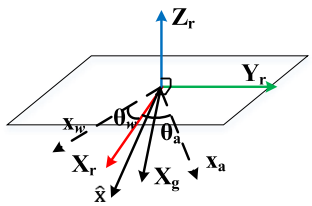

Fig. 6. Lateral direction estimation. X_a is an estimation of X_g derived from the acceleration. X_w is an estimation of X_g derived from the angular velocity. $\widehat{X}$ is a hybrid estimation from X_a and X_w.

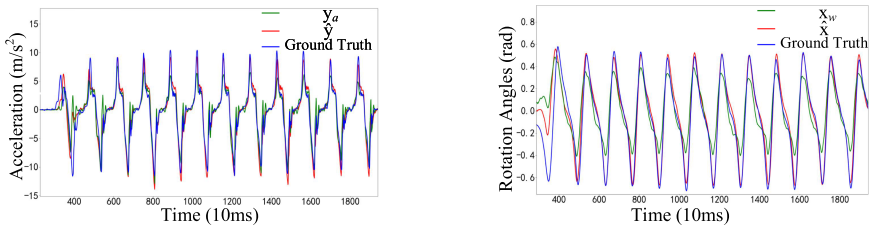

(a) Acceleration (b) Rotation Angles

Fig. 7. PCA results vs. ground truth.

IMU can be calculated as follows:

$$\mathbf{R_{rg}} = \begin{bmatrix} \cos\widehat{\theta} & \sin\widehat{\theta} & 0 \\ -\sin\widehat{\theta} & \cos\widehat{\theta} & 0 \\ 0 & 0 & 1 \end{bmatrix}. \tag{7}$$

The quaternion $\mathbf{q_{lr}(t)}$ can be expressed as rotation matrix $\mathbf{R_{lr}(t)}$ according to Reference [5]. Therefore, the transformation from IMU's LCS at time t to GCS can be expressed in rotation matrix formation as $\mathbf{R_{lr}(t)R_{rg}}$. Thus, each IMU at every sampling time can align its LCS to GCS.

To evaluate the performance of the PCA-based solution, we conduct an experiment when the subject is walking along a straight line. Specifically, we plot the PCA results from the *acceleration-based method*, i.e., y_a, as well as the PCA results from the *hybrid method*, i.e., $\widehat{y}$, and compare with the ground truth in Figure 7(a). The correlation between the ground truth and y_a result is around 0.875, and the correlation between the ground truth and $\widehat{y}$ result is around 0.941. We also plot the PCA results from the *angular velocity-based method*, i.e., y_w, as well as the PCA results from the *hybrid method*, i.e., $\widehat{y}$, and compare with the ground truth in Figure 7(b). The correlation between the ground truth and x_w result is around 0.900, the correlation between the ground truth and $\widehat{x}$ result is around 0.923. It shows that the PCA-based solution can accurately derive the forward direction and the lateral direction; moreover, the *hybrid method* can further improve the performance in forward/lateral direction estimation.

4.2 Estimation of Lower Limb Length

Next, we introduce how to estimate the lower limb length based on the stride length. *Stride length*, *step length*, and *step width* are common and important spatial parameters in gait analysis. As shown in Figure 8(a), the *stride length d* is the distance between successive ground contacts of the same foot along the forward direction, the *step length s* is the distance along the forward direction between the heel contact point of one foot and that of another foot, and the *step width w* is the distance along the lateral direction between the heel contact point of one foot and that of another foot.

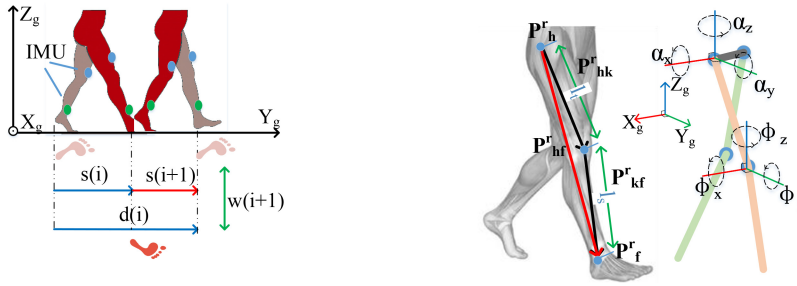

(a) Spatial gait parameters: stride length, step length and step width

(b) Compute step length and step width from geometri model

Fig. 8. The stride length calculated by geometric model.

In principle, they can be estimated by tracking the positions of IMUs near left and right feet. However, since small errors in linear acceleration may accumulate large errors after double integration, it is difficult to accurately estimate the positions of IMUs, especially when we calculate the relative positions of multiple IMUs. For *stride length d*, we can still estimate it by double integrating linear acceleration of only one IMU near the foot over a gait cycle. The reason is that the error in estimating d can be limited, since it only needs to double integrate the acceleration of one IMU within a small time window. However, it is hard to calculate *step length* and *step width*, because they are relative to the positions of two IMUs. Nevertheless, since we can obtain the rotation angles of IMUs around X_g, Y_g, and Z_g based on the rotation matrix of LCS to GCS, it provides us a new opportunity to calculate *step length* and *step width* according to the geometric model of human body [22]. As shown in Figure 8(b), we can infer the positions of knees and feet relative to hips based on the rotation angles around X_g and Y_g, thigh length l_t, and shank length l_s.

Based on the understanding, we need to first obtain the thigh length l_t and shank length l_s and then estimate the corresponding gait parameters. Based on observation 2, the *stride length* calculated from acceleration should be equivalent to the result calculated from the geometric model. Hence, we build a regression model between l_t, l_s, rotation angles of thighs α, rotation angles of shanks ϕ, and the *stride length d*. Then we can infer l_t and l_s from this model.

4.2.1 Stride Length Estimation from Geometric Model. We first propose to estimate the *stride length* according to the geometric model. As shown in Figure 8(a), the ith stride length $d(i)$ is the sum of two consecutive step lengths $s(i)$ and $s(i+1)$. For each step length $s(i)$, it is the distance between two feet on the forward direction when one foot's toes are about to leave the ground. Thus, we build the geometric model shown in Figure 8(b), which is a snapshot of lower limbs when the toes are about to leave the ground. In this model, assuming that the positions of hips are known, let the rotation angles of thighs and shanks be α and ϕ, respectively, we can calculate the positions of feet based on the geometric model. Recall that based on the IMUs attached on thighs and shanks, we can obtain the rotation matrix converted from LCS to GCS aforementioned in Section 4.1. With the rotation matrix, the corresponding Euler angles can be inferred as in Reference [5] as the rotation angles.

We take the right foot as an example. Here, we use the superscript to distinguish the right leg from the left one. As shown in Figure 8(b), the position of right hip is $\mathbf{p}^{\mathbf{r}}_{\mathbf{h}}$, the thigh length is l_t, and the shank length is l_s. For the ith step, the rotation angle of thigh is $\alpha^r(i)$ and the rotation angle of shank $\phi^r(i)$. Then, we can extract the rotation angle around X_g axis as $\alpha^r_x(i)$ and $\phi^r_x(i)$, respectively, and extract the rotation angle around Y_g axis as $\alpha^r_y(i)$ and $\phi^r_y(i)$, respectively. Therefore, the

position vector of right foot relative to right hip $\mathbf{p}^{\mathbf{r}}_{\mathbf{hf}}$ can be expressed as follows:

$$\mathbf{p}^{\mathbf{r}}_{\mathbf{hf}} = \mathbf{p}^{\mathbf{r}}_{\mathbf{hk}} + \mathbf{p}^{\mathbf{r}}_{\mathbf{kf}}. \tag{8}$$

Here, $\mathbf{p}^{\mathbf{r}}_{\mathbf{hk}}$ is the position vector of right knee relative to right hip and $\mathbf{p}^{\mathbf{r}}_{\mathbf{kf}}$ is the position vector of right foot relative to right foot. $\mathbf{p}^{\mathbf{r}}_{\mathbf{hk}}$ and $\mathbf{p}^{\mathbf{r}}_{\mathbf{kf}}$ can be expressed by thigh length and rotation angles as

$$\mathbf{p}^{\mathbf{r}}_{\mathbf{hk}} = l_t \begin{bmatrix} -\sin \alpha^r_y(i) \\ \cos \alpha^r_y(i) \sin \alpha^r_x(i) \\ -\cos \alpha^r_x(i) \cos \alpha^r_y(i) \end{bmatrix}, \tag{9}$$

$$\mathbf{p}^{\mathbf{r}}_{\mathbf{kf}} = l_s \begin{bmatrix} -\sin \phi^r_y(i) \\ \cos \phi^r_y(i) \sin \phi^r_x(i) \\ -\cos \phi^r_x(i) \cos \phi^r_y(i) \end{bmatrix}. \tag{10}$$

Similarly, we can also figure out the position vector of left foot relative to left hip.

Since the step length is the distance between two feet on the Y_g axis, the left and right hips have the same coordinates on the Y_g axis. The ith step length $s(i)$ can be then estimated as follows:

$$\begin{aligned} s(i) =& |l_t(\cos \alpha^r_y(i) \sin \alpha^r_x(i) - \cos \alpha^l_y(i) \sin \alpha^l_x(i)) \\ &+ l_s(\cos \phi^r_y(i) \sin \phi^r_x(i) - \cos \phi^l_y(i) \sin \phi^l_x(i))|. \end{aligned} \tag{11}$$

Thus, the length of ith stride $d(i)$ can be calculated as follows:

$$d(i) = s(i) + s(i+1). \tag{12}$$

4.2.2 Stride Length Estimation from Acceleration. Instead of calculating the *stride length* from the geometric model, the *stride length* can also be calculated as the displacement of one identical IMU attached on the shank. Since continuous integrating acceleration may lead to a huge error, we segment the time-series acceleration and integrate the acceleration in each segment. Therefore, the estimation can be divided into two steps: *gait cycle segmentation* and *stride length estimation*.

Gait cycle segmentation is based on the rotation angles of shank around X_g, i.e., ϕ_x. Figure 9(a) shows the process of a typical gait cycle. During the process, the ϕ_x turns from positive to negative when the foot touches the ground completely, as shown in Figure 9(b). Therefore, we can segment the acceleration into gait cycles by calculating the *zero crossing point* of the rotation angles.

For each segment, its corresponding stride length can be calculated by double integrating acceleration from the start time t_s to the end time t_e of the segment. Supposing the measured acceleration is $\widehat{\mathbf{a_g(t)}}$, we first calculate the velocity $\mathbf{v(i)}$ by integrating the acceleration as

$$\mathbf{v(i)} = \int_{t_s}^{i} \widehat{\mathbf{a_g(t)}} dt. \tag{13}$$

Ideally, $\mathbf{v(t_e)}$ is zero, since t_e corresponds to the time when foot touches the ground completely. However, $\mathbf{v(t_e)}$ is not zero due to the error $\mathbf{e(t)}$ in $\widehat{\mathbf{a_g(t)}}$, as shown in Figure 9(c). Therefore, we introduce *Zero Velocity Calibration* to reduce the error. We assume that the $\mathbf{e(t)}$ is a constant and calibrate the acceleration as follows:

$$\mathbf{e(t)} = \frac{\mathbf{v(t_e)}}{t_e - t_s}, \tag{14}$$

$$\mathbf{a_g(t)} = \widehat{\mathbf{a_g(t)}} - \mathbf{e(t)}. \tag{15}$$

Then the displacement $\mathbf{d(i)}$ can be estimated by quadratic integration of acceleration $\mathbf{a_g(t)}$. Finally, we can obtain $\mathbf{d(t_e)}$ on Y_g axis as the stride length.

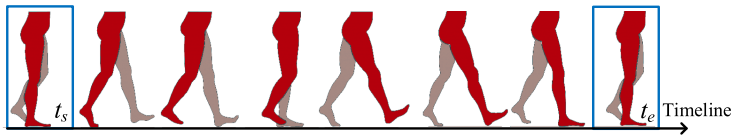

(a) Gait Cycle.

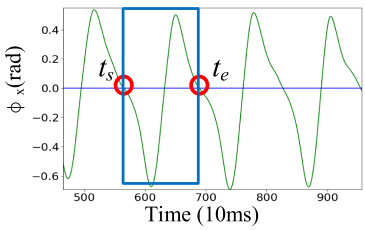

(b) Cycle Segmentation.

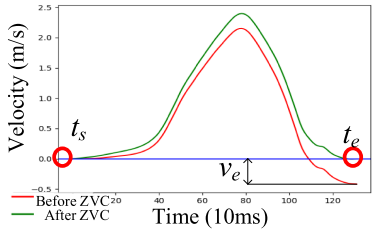

(c) Zero Velocity Calibration.

Fig. 9. Segment gait cycles based on the rotation angles of thighs around X_g. Calibrate acceleration within a segment by zero velocity calibration.

4.2.3 Lower Limbs Length Estimation Model. Since the *stride length* can be calculated from the linear acceleration and the geometric model, respectively, the results obtained by these two methods are theoretically consistent. Therefore, we combine the two methods of stride length estimation and introduce a regression model to estimate l_t and l_s:

$$l_t, l_s = \underset{l_t, l_s}{\operatorname{argmin}} \sum_{i=0}^{n} (s(i) + s(i+1) - d(i))^2. \tag{16}$$

Here, $d(i)$ is the length of ith stride calculated from acceleration and $s(i)$ and $s(i+1)$ are lengths of two steps in the ith stride calculated from geometric model. Based on the estimated stride length, we can obtain the lengths of thighs and shanks, i.e., l_t and l_s. The length of the lower limbs can be further used to calculate other gait parameters.

4.3 Shift of Origin for Each IMU

After we perform the estimation of the lower limb length, including the thigh length and shank length, we can estimate the shift of origin for each of the IMUs based on either the geometric model or the acceleration measurement in the GCS. Specifically, on the one hand, according to the geometric model with the knowledge of the thigh length and shank length, GaitTracker can effectively estimate the shift of origin for each of the IMUs, based on the angle measurement from the gyroscopes in the IMU. On the other hand, the shift of origin for each of the IMUs can also be estimated by directly calculating acceleration measurement in the unified and synchronized GCS.

5 SYSTEM DESIGN

GaitTracker consists of three modules: *Data Collection*, *Feature Extraction*, and *Gait Monitoring*. As shown in Figure 10, *Data Collection* module collects motion data including the linear accelerations and rotation angles. *Feature Extraction* module extracts the gait features from raw motion data. *Gait Monitoring* module estimates the specified gait parameters and performs 3D skeletal tracking, including the rotation and displacement of the lower limbs, according to the extracted gait features. Conventionally, the *Data collection* module is implemented locally in the IMU sensors. The *Feature*

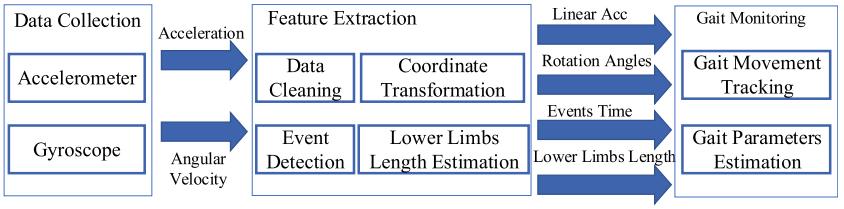

Fig. 10. System overview.

Extraction module can be implemented either locally in the mobile device or remotely in the server, which depends on the processing capability of the mobile device. Then the raw sensor data or the gait features can be uploaded to the server via the mobile device. *Gait Monitoring* module can be implemented in the server. The end users such as the rehabilitation specialists can use the APPs in the smart phone or the browsers in the PC to access the GUI of *Gait Monitoring* module.

5.1 Data Collection

As shown in Figure 2(a), GaitTracker has four IMUs, one **MicroController Unit (MCU)**, one bluetooth agent, and a power bank. IMUs are deployed on the thighs and shanks of the two legs with straps to measure acceleration and angular velocity. The sampling rate is set to 100 Hz by default. The MCU collects motion data, including acceleration and angular velocity, and then forwards the data to a Bluetooth-paired smartphone. A rechargeable power bank is used to power the entire system.

5.2 Feature Extraction

Feature Extraction module is designed to extract the metadata from the original motion signal to achieve the gait monitoring, including the motion signal in the GCS, the occurrence time of key events in the gait cycle, and the length of the lower limbs.

5.2.1 Data Cleaning. After collecting motion data from the MCUs, we first clean the data by removing high-frequency noise and canceling the measurement offset. Since the noise of electronic components is concentrated on the high frequencies, a low-pass filter is used to remove the high-frequency noise. For the offset, because the gyroscope measurements are ideally equal to zero when the IMU is static, before the user performs gait rehabilitation, we ask the subject to stand still for 5 s and calculate the signal offset for canceling.

5.2.2 Coordinate Transformation. As aforementioned in Section 4.1.1, we need to transform the motion data from the LCS to the GCS. First, when the user stands still for offset estimation, we can use the corresponding motion data to build the RCS and calculate the rotation matrix from LCS to RCS, according to Section 4.1.1. Then we further transform RCS to GCS when the subject starts walking along a straight line, which can provide a consistent fluctuation among all the IMUs for space synchronization. Since the subject usually walks forward and backward along a straight line for gait rehabilitation, without loss of generality, we just consider the two walking directions. For the forward direction, we directly use the algorithm in Section 4.1.2 to align all the IMUs to GCS. For the backward direction, we just replace θ with $\theta + \pi$ in Equation (7) and then align all the IMUs to GCS similarly. The direction change can be determined by integrating angular velocity along Z_r during one step length. If this angle approaches π, then it means the subject turns backward. If the subject turns to other directions, then we can also update the GCS after the turning and transform the RCS to the updated GCS, similarly.

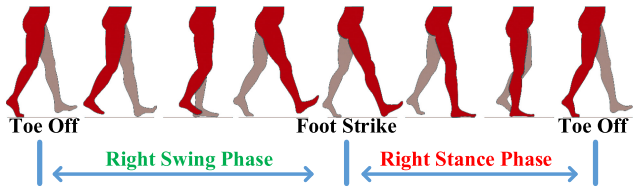

Fig. 11. Gait cycle.

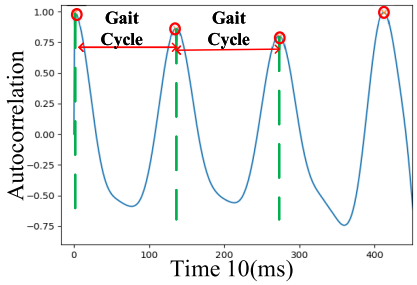

Fig. 12. Gait cycle estimation by calculating the distance between peaks of autocorrelation of acceleration.

5.2.3 Gait Cycle and Phase Detection. A *gait cycle* is the time period between the ground contact of one foot and the subsequent contact of the same foot [2]. Each gait cycle has two phases: *stance phase* and *swing phase*. *Stance phase* is the period during which the target foot contacts with the ground and the *swing phase* is the period during which the target foot is swinging in the air. As shown in Figure 11, we can detect the occurrences of the **toe off (TO)** and **foot strike (FS)** [13] events to segment the stance phase and swing phase. Here, TO is used to detect the beginning and ending of each gait cycle, and FS is used to split one gait cycle into *swing phase* and *stance phase*.

We use the motion signal of IMUs to estimate the gait cycle and detect the two events according to the gait cycle. Because the gait cycles are periodic, we calculate the pitches as the rotation angles around X_g in GCS and use the autocorrelation coefficient of pitches to estimate the gait cycle as shown in Figure 12. Gait cycle duration t_g can be estimated by the average of interval between the peaks in autocorrelation coefficient.

For the TO point, it is corresponding to the moment when the thighs swing backward the most. Therefore, we determine the TO points from the valleys of pitches of IMUs attached on the thighs as shown in Figure 13(a). Due to the periodical feature, false detection of valleys can be efficiently filtered out based on the gait cycle t_g. Due to the periodical feature, we detect the TO points as the minimum valleys of pitches in the window of size $\tau \cdot t_g$; τ is an empirical parameter and we set τ as $\frac{2}{3}$.

For the FS point, it occurs when the foot first strikes. The height of the IMU decreases before the FS event and increases after the FS event. Here, the height of IMU, i.e., the displacement in the Z_g, is obtained from a double integration on the linear acceleration in the Z_g. Therefore, the FS point is detected as the valley of the IMU's height, as shown in Figure 13(b).

5.2.4 Lower Limbs Length Estimation. According to the model in Section 4.2.3, we can estimate the lower limb length from the stride length and the joint rotations. For the stride length, we collect the linear acceleration in GCS of IMUs attached on shanks and calculate it as the displacement of IMU during the time period from the TO event to the FS event in each gait cycle. Particularly, we

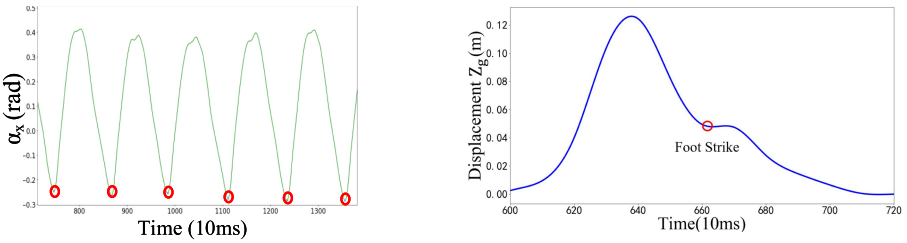

(a) Toe Off. (b) Foot Strike.

Fig. 13. Phase detection.

use *Zero Velocity Calibration* to remove errors in acceleration. The displacement can be estimated by double integrating the calibrated acceleration.

Besides, the stride length can also be calculated by summing up two step lengths in one stride. Each step length can be expressed as a function of the length of thighs and shanks and rotation angles of thighs and shanks when TO happens. Thus, we collect the rotation angles of thighs and shanks at the moments of two TO events and use the rotation angles to calculate the length of lower limbs. We estimate the length of lower limbs over all the stride cycles during the gait rehabilitation process and then use the average value as the final estimate.

5.3 Gait Monitoring

After extracting the features, we obtain the linear acceleration $\mathbf{a_g}$ in GCS, the rotation angles of thigh α and shank ϕ, the length of thigh l_t and shank l_s, and the occurrence time of TO and FS. Based on these extracted features, we can track the movement and further estimate gait parameters.

5.3.1 Gait Movement Tracking. Gait movement tracking is to track the rotation and position of a human subject's lower limbs. For the rotations, we can calculate them from the rotation matrix between GCS and LCS. For the positions, since one of the two feet touches on the ground at any time during the gait rehabilitation, we can treat this foot as the anchor and calculate the positions of other limbs from the rotation angles of each joint based on the geometric model as shown in Figure 8.

Suppose that the right foot is on the ground for the ith step, and we obtain the corresponding position of this foot. Then in the consecutive time, we can obtain the rotation angles of both the right thigh and shank as well as the left thigh and shank. As shown in Figure 14, assume that the left and right hips share the same position or have a fixed space length, then we can regard the right foot as an anchor and leverage the geometric model to calculate the position of each joint until the FS event of left foot happens. When the FS event of left foot happens, the left foot starts to stand on the ground. Then we can further take the left foot as the anchor and calculate the other joint positions. Finally, we can track the gait movement by treating one of the two feet as the anchor alternately.

5.3.2 Gait Parameters Estimation. In addition to gait movement tracking, GaitTracker also calculates the gait parameters according to the features extracted from motion data.

Stride Length is the distance between successive heel contact points of the same foot along the forward direction, as shown in Figure 8(a). We segment the acceleration on Y_g based on the TO event and then apply Zero Velocity Calibration in Section 4.2.2 and double integrate the acceleration to calculate the stride length.

Step Length is the distance between the heel contact point of one foot and that of another foot along the forward direction, as shown in Figure 8(a). Based on the model in Section 4.2.1, the step

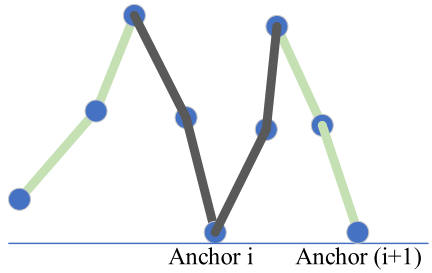

Fig. 14. Gait movement tracking.

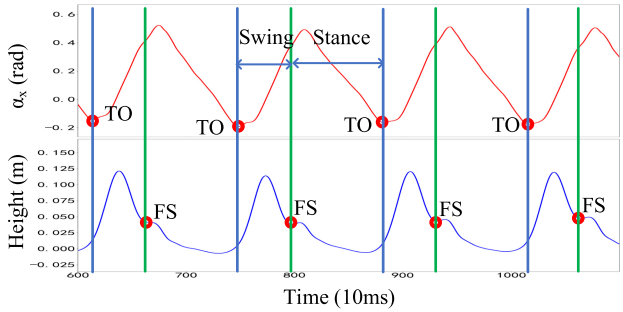

Fig. 15. Gait phase segmentation.

length can be calculated as $|\mathbf{p}^{\mathrm{l}}_{\mathrm{hf}} - \mathbf{p}^{\mathrm{r}}_{\mathrm{hf}}|_y$, where $\mathbf{p}^{\mathrm{l}}_{\mathrm{hf}}$ is the position vector from left hip to left foot and $\mathbf{p}^{\mathrm{r}}_{\mathrm{hf}}$ is the position vector from right hip to right foot.

Step Width is the distance between the heel contact point of one foot and that of the other foot along the lateral direction, as shown in Figure 8(a). Step width is calculated similarly to the step length, as $|\mathbf{p}^{\mathrm{l}}_{\mathrm{hf}} - \mathbf{p}^{\mathrm{r}}_{\mathrm{hf}}|_x$.

Cycle Time is the time between successive foot contacts of the same foot. Assuming the ith time of TO event is $t_{TO}(i)$, the cycle time is $t_{TO}(i) - t_{TO}(i-1)$, as shown in Figure 15.

Swing Time is the period of the gait cycle during which the foot is in the air. Assuming the time of FS between $t_{TO}(i)$ and $t_{TO}(i+1)$ is $t_{FS}(i+1)$, the swing time is $t_{FS}(i+1) - t_{TO}(i)$, as shown in Figure 15.

Stance Time is the period of the gait cycle during which the foot touches the ground. Similarly to the swing time, the stance time can be calculated by $t_{TO}(i) - t_{FS}(i)$, as shown in Figure 15.

Knee Joint Angles are the angles between the thighs and shanks. Knee joint angles can be calculated by $\alpha - \phi$.

Symmetry [17] is used to delineate the differences of gait movements of two limbs. Symmetry is calculated based on the following equation:

$$Symmetry = 100 * \frac{abs(M_l - M_r)}{0.5 * (M_l + M_r)}, \tag{17}$$

where M is the step length or swing time of left or right limb.

6 PERFORMANCE EVALUATION

6.1 Experimental setup

We fully implement *GaitTracker*, which consists of four *MPU*9250 IMUs, an *STM*32*F*103*C*8 MCU, and an *FBT*06 Bluetooth module, as shown in Figure 2(a). As shown in Figure 16, during our

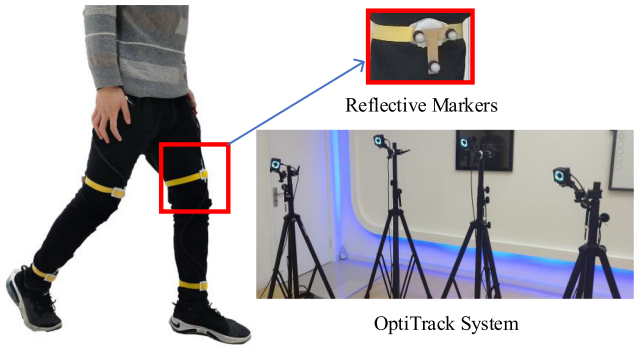

Fig. 16. The experimental setup.

experiments, GaitTracker is attached to a human subject on her/his lower limbs to track the 3D skeletal gait movements and estimate the corresponding gait parameters. An OptiTrack System is deployed to collect the ground truth. Specifically, three reflective markers are attached on each one of the IMU sensors, and thus in total $4 \times 3 = 12$ markers are used. Four OptiTrack cameras are deployed in the indoor environment to track the 3D position of the reflective markers as ground truth. Since the monitoring area of OptiTrack is fairly limited, during the evaluation process, we let the human subject walk in a straight line in a back and forth manner. In this way, the experiment can be effectively set up to capture the ground truth of gait movements. To evaluate the performance of *GaitTracker*, we conduct several experiments to examine the performance of coordinate transformation, estimation of lower limb length, gait movement tracking and gait parameters estimation in realistic settings.

6.2 Performance of Coordinate System Transformation

Since the rotation representation of quaternion and rotation matrix is not intuitive, we convert it to Euler angles to evaluate the performance of coordinate system transformation. We use s1, s2, s3, and s4 to represent the sensors on the left shank, right shank, left thigh, and right thigh, respectively. For transformation from LCS to RCS, 10 human subjects are given an instruction to walk in a straight line at a moderate speed (1 m/s) for 30 s, repeating 10 times. We compare the extracted angle error of our algorithm with the *Kalman filter* [4] and the ordinary *gyroscope tracking* algorithm [30], based on the sensors attached on the different positions. As shown in Figure 17(a), the results show that our *adaptive complementary filtering* algorithm achieves very close accuracy to Kalman filter, with an error of about 3°. Moreover, the error of gyroscope tracking algorithm drifts with time, and the drift becomes larger over time. We also evaluate the tracking performance when walking at different speeds. Particularly, a subject walks at a low speed of 0.5 m/s, a medium speed of 1 m/s, and a high speed of 1.5 m/s. The error of the sensor on thigh is shown in Figure 17(b). The results show that our *adaptive complementary filter* algorithm maintains a calculation error of about 3° at different speeds.

For transformation from RCS to GCS, we use the angle between X_r and X_g as the evaluation metric. As shown in Figure 17(c), the error of our method is around 1.5°. As a comparison, the error of *magnetometer-based solution* is around 12.4°. We also consider the performance at different walking speed as show in Figure 17(d). As the speed increases, the error of our solution increases slightly, but remains around 2°. However, the errors of *magnetometer-based solution* are all above 12° in all the situations. The reason of the large error of a magnetometer-based solution is due to the issue of unstable magnetic field in the indoor environment. Specifically, magnetometer

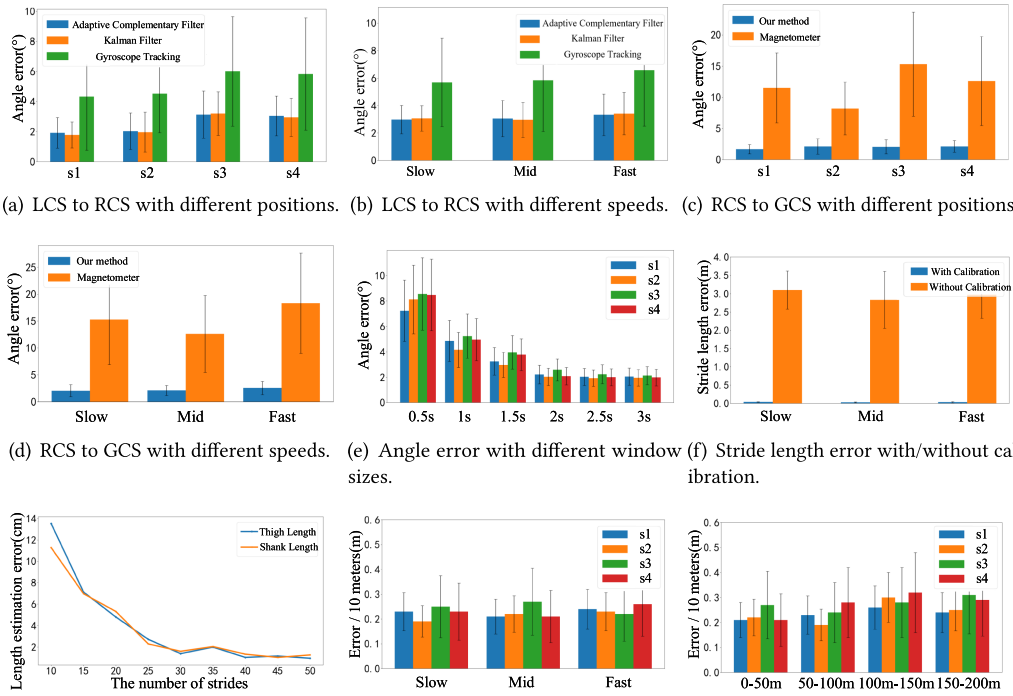

(a) LCS to RCS with different positions. (b) LCS to RCS with different speeds. (c) RCS to GCS with different positions.

(d) RCS to GCS with different speeds. (e) Angle error with different window sizes. (f) Stride length error with/without calibration.

(g) Length estimation error with the number of strides (h) Displacement estimation error with different speeds. (i) Error drift of displacement estimation.

Fig. 17. Performance evaluation.

readings are often notoriously inaccurate in indoor environments, due to the magnetic interference caused by the massive steel embedded in building concrete structures and other metallic objects. Therefore, when the user walks to different positions in the indoor environment, the indoor magnetic field may vary from position to position and be susceptible to the surrounding environment. Hence, the magnetometer-based solution cannot identify a consistent direction to synchronize the coordinates of different IMU sensors. In contrast, our system accurately synchronizes the coordinates, outperforming the *magnetometer-based solution*.

Moreover, we compare the performance of different window sizes. As shown in Figure 17(e), when the window size increases from 0.5 to 2 s, the errors of all four sensors decrease dramatically. After that, the increment of the window size has little impact on the performance, because 2 s of window is enough to calculate the direction of the global coordinate system.

6.3 Performance of Lower Limbs Length Estimation

Before validating the estimation of lower limb length, we first verify the accuracy of stride length calculation with zero velocity calibration. Similarly, 10 human subjects are given an instruction to walk in a straight line at a moderate speed (1 m/s) for a minute and calculate the stride length from the sensing data. We further calculate the error by comparing with the ground truth. As shown in Figure 17(f), the error of calculation with zero velocity calibration is around 3 cm. As a comparison, the error of calculation without zero velocity calibration is almost 3 m. This is because when the velocity is not calibrated, the error accumulates rapidly, which leads to large accumulative error.

After calibration, the error of each stride will not affect the next stride, which ensures that the error will not accumulate over time. Then, we further evaluate the performance of lower limb

Table 2. Gait Paramters Estimation

Gait Paramters	Left lower limb				Right lower limb			
	estimation	ground truth	error	percentage error	estimation	ground truth	error	percentage error
Stride length (m)	1.23	1.25	−0.02	1.6%	1.21	1.24	−0.03	2.4%
Step length (m)	0.67	0.66	0.01	1.5%	0.66	0.68	−0.02	2.9%
Step width (cm)	3.78	4.21	0.43	10.2%	3.84	4.35	0.51	11.7%
Cycle time (s)	1.22	1.20	0.02	1.7%	1.24	1.21	0.03	2.5%
Swing time (s)	0.46	0.47	−0.01	2.1%	0.47	0.48	−0.01	2.1%
Stance time (s)	0.76	0.73	0.03	3.9%	0.74	0.73	0.01	1.4%
Knee joint angle (deg)	—	—	1.17	—	—	—	1.32	—

length estimation based on the same sensing data of the stride length estimation. As shown in Figure 17(g), as the subject walks forward over time, the estimation scheme gradually obtains enough training data, the estimation error of thigh and shank length gradually converges to a fixed value, e.g., it is around 1.5 cm after the number of strides is over 40. The result shows that *GaitTracker* accurately calculates the length of lower limbs after a certain number of strides, e.g., 40 strides.

6.4 Performance of Gait Tracking

We evaluate the gait tracking by examining the accuracy of rotation angles and the displacement calculation. Since the rotation angles are calculated from the coordinate system transformation in Section 6.2, we only evaluate the accuracy of displacement calculation. Particularly, 10 human subjects are given an instruction to walk at three different speeds, and we calculate the rotation angles and the displacements. As shown in Figure 17(h), the displacement calculation of the sensor at the shanks and thighs has an average error of 0.23 m and 0.24 m for every 10 m, respectively.

We further evaluate the error drift of the displacement calculation. We ask the subjects to walk at a moderate speed (1 m/s) for 200 m. Then we divide the displacement into four segments and evaluate the calculation error of each segment. As shown in Figure 17(i), the error accumulates slightly over time but the cumulative speed is small. Considering that it is difficult to completely eliminate the error of displacement calculation only by inertial sensor, the small cumulative speed already satisfies the demand in the field of gait monitoring.

6.5 Performance of Gait Parameter Estimation

Finally, we compare the gait parameter estimated from GaitTracker with the ground truth obtained from OptiTrack so as to evaluate the performance of gait parameter estimation. We ask the subjects to walk with a normal posture, and the statistical results are shown in Table 2. The estimation errors of most parameters are maintained at about 3% except for the step width. Because the ground truth of the step width itself is small, the error percentage is about 10%. For the knee joint angle, the error is around 1.5°. The results indicate that *GaitTracker* accurately estimates the gait parameters even though the subject only walks for a small distance.

7 CASE STUDY

7.1 System Design and Real Deployment

We implemented a remote gait monitoring system for GaitTracker and further performed case study in real applications. Figure 18 shows the main components of the system: (1) *Perception Module* is provided for the patients, which includes a wearable kit shown in Figure 2(a) for motion data collection, as well as a mobile application to transmit the data to the cloud server, as shown in

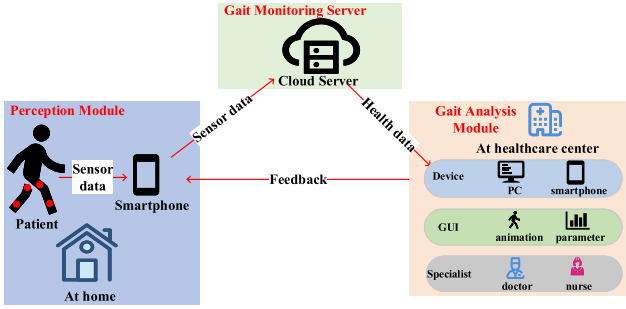

Fig. 18. Remote gait monitoring system.

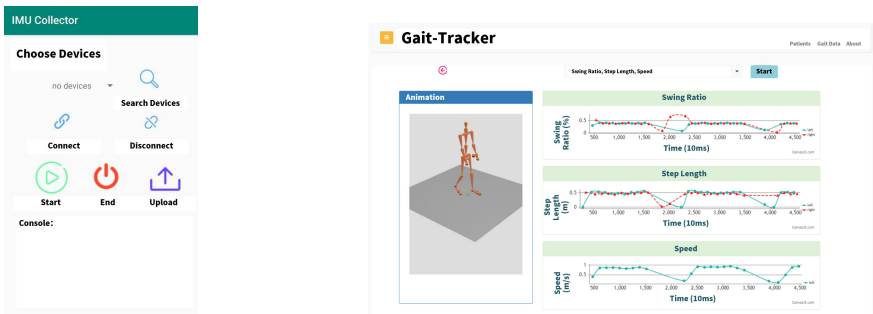

(a) GUI of Perception Module (b) GUI of Gait Analysis Module

Fig. 19. Graphical user interface of GaitTracker system.

Figure 19(a). (2) *Gait Monitoring Server* extracts the gait features from the raw sensing data on the cloud server, which are further used to track the gait movement and estimate the gait parameters. (3) *Gait Analysis Module* reconstructs the gait animation and displays the charts of gait parameters for specialists to analyze on the web, as shown in Figure 19(b).

We deployed the system in a rehabilitation center and evaluated the system with different kinds of patients. Specifically, the patients with normal gait, hemiplegic gait, and quadriceps gait were invited to evaluate the system performance. Figure 20 shows the different gait animations reconstructed by our system. For the animations of normal gait in Figure 20(a), the movements of the lower limbs are symmetrical. For the animations of hemiplegic gait in Figure 20(b), the motion of right leg circumduction is clearly displayed. For the animations of quadriceps gait in Figure 20(c), the height and step length of the right foot are obviously lower than the normal gait.

7.2 Gait Parameter Measurement

We compare the rotation angles around X_g axis and Y_g axis, respectively, for the corresponding gaits in Figure 21. For the *normal gait*, as shown in Figure 21(a), the rotation angles of normal gait have obvious symmetry and periodicity. For the *hemiplegic gait*, as shown in Figure 21(b), the period duration of a whole gait cycle is longer than that of the normal gait. Besides, the waveform of the normal and trouble sides is significantly different. The maximum rotation angles of the trouble side around X_g axis is significantly smaller than that of the normal side, because the step length of the trouble side is shorter than that of the normal side. In addition, the rotation angle of the trouble side around Y_g axis is larger than that of the normal gait, which corresponds to the leg circumduction. For the *quadriceps gait*, as shown in Figure 21(c), the waveform of the normal side is similar to that of the hemiplegic gait. The maximum rotation angles of the trouble side around

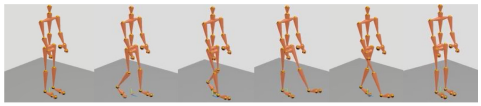

(a) Normal Gait.

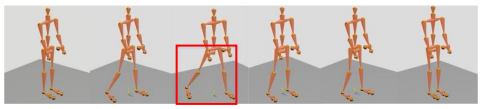

(b) Hemiplegic Gait.

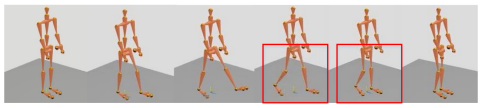

(c) Quadriceps Gait.

Fig. 20. Gait Animations.

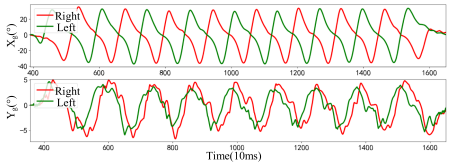

(a) Normal Gait.

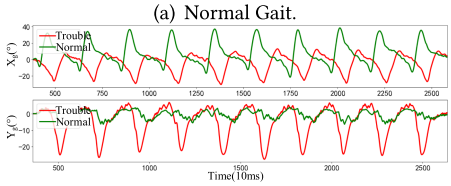

(b) Hemiplegic Gait.

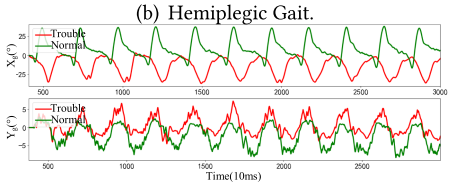

(c) Quadriceps Gait.

Fig. 21. Rotation angles of shanks around X_g and Y_g.

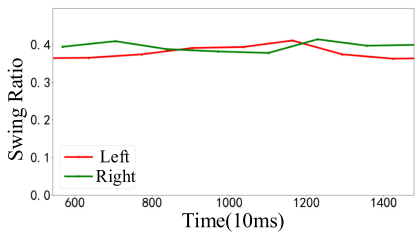

(a) Normal Gait.

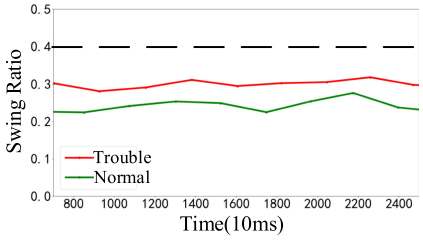

(b) Hemiplegic Gait.

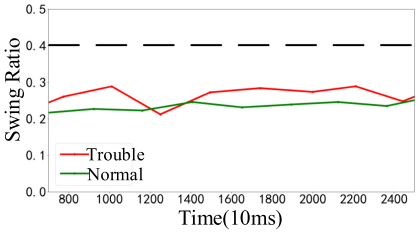

(c) Quadriceps Gait.

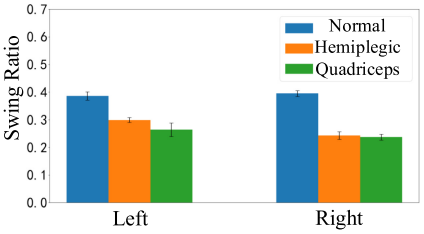

(d) Compare Swing Ratio.

Fig. 22. Swing ratio of different gaits.

X_g axis are close to zero, which corresponds to the dragging posture. Besides, the step length of the trouble side is small. Compared with the previous two gaits, the jitter of the rotation angles around Y_g axis is more obvious. Therefore, the rehabilitation specialists can track the patient's gait movement by our system, and the recovery gait animation is consistent with the movement observed from the cameras.

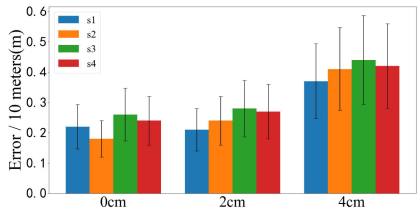

(a) Displacement Error with IMU Position Deviations

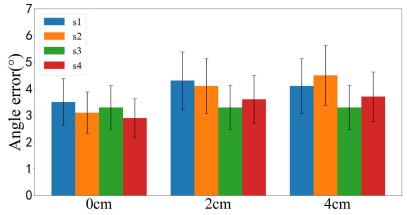

(b) Angle Error with IMU Position Deviations

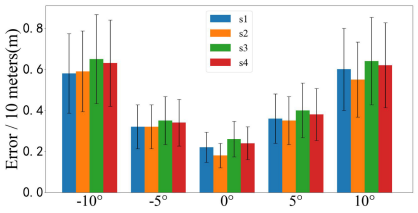

(c) Displacement Error with IMU Rotation Deviations

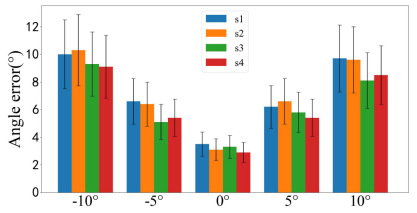

(d) Angle Error with IMU Rotation Deviations

Fig. 23. Robustness evaluation with different deviations of IMU rotation and position.

For the estimation of gait parameters, we investigate the *swing ratio* (swing time/cycle time) as an example in Figure 22. For the *normal gait*, as shown in Figure 22(a), the difference of swing ratio between the left and right limbs is small and the swing ratio is around 0.4, which is consistent with the normal medical parameters. For the *hemiplegic gait*, as shown in Figure 22(b), the swing ratio of two sides is obviously lower than 0.4 due to the decrement of patient's balance. In addition, the swing ratio on the trouble side is higher than that on the normal side, because the patient is eager to transfer the weight to the normal side. For the *quadriceps gait*, as shown in Figure 22(c), the swing ratio of two sides is also lower than 0.4 due to the decrement in patient's balance. Figure 22(d) compares the swing ratio of different gaits. We find that the swing ratio of abnormal gaits is obvious lower than normal gait, and this is consistent with clinical observation. In conclusion, *GaitTracker* can accurately track the gait movement and estimate the gait parameters.

7.3 Robustness Evaluation

During the process of walking, the IMU sensors' wearing positions could be changed or rotated along the leg to a certain degree, and we thus evaluate how the system performance will be impacted due to these issues. We first change the position deviation to different values from 0, 2, and 4 cm, then we let the human subject walk for 10 m, and evaluate the displacement error and angle error of the gait trace, in comparison to the ground truth. Figure 23(a) and (b) show the experiment results. Here, we use s_1, s_2, s_3, and s_4 to respectively denote the IMU sensor on left shank, right shank, left thigh, and right thigh. We can find that both the displacement error and angle error can be effectively restricted in a small range. Specifically, the displacement errors are all below 0.5 m, and the angle errors are all below 5°. We further change the rotation deviation to different values from 0°, 5°, and 10°, then we let the human subject walk for 10 m and evaluate the displacement error and angle error of the gait trace. As shown in Figure 23(c) and (d), the displacement errors are all below 0.7 m, and the angle errors are all below 10°. As a matter of fact, since

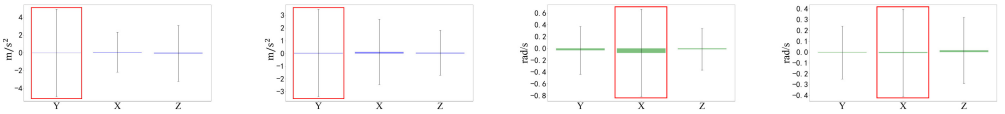

(a) Acceleration of Shank (b) Acceleration of Thigh (c) Gyroscope of Shank (d) Gyroscope of Thigh

Fig. 24. Robustness evaluation of forward direction estimation for feet-dragging case.

in real deployment we can use the wearable design like the elastic knee cap to prevent or mitigate the position/angle deviation, the corresponding displacement error and angle error can be greatly reduced.

Note that when in rehabilitation, people's feet-dragging characteristic can deviate significantly from normal state, it is not yet clear how the performance in forward direction estimation will be impacted by this issue. In this situation, to evaluate the performance of PCA-based method to determine the forward direction, we let the patients with hemiplegic gait walk along the Y_g axis for 20 s and further evaluate the mean and standard deviation of linear acceleration and angular velocity in different axes of the global coordinate. The experiment results are shown in Figure 24. Similarly to Figure 3, we find that, despite the feet-dragging characteristic in the hemiplegic gait, the fluctuation of acceleration is still concentrated on the forward direction, i.e., Y_g, and the fluctuation of angular velocity is still concentrated on the lateral direction, i.e., X_g in the global coordinate system. This means that the feet-dragging characteristic does not significantly impact the performance in forward direction estimation.

8 CONCLUSION

In this article, we propose *GaitTracker*, a wearable system to remotely and continuously perform gait monitoring and analysis by 3D skeletal tracking. We attach four IMUs on the shanks and thighs of the human body to collect motion data, track the gait movement, and estimate the gait parameters. We design several novel algorithms to adaptively synchronize the coordinate systems of different IMUs and reconstruct the gait movements based on the geometric model of lower limbs. Furthermore, we extract the gait parameters from the gait movement without any prior knowledge, which can be directly used to evaluate the gait rehabilitation. We implement a prototype system of *GaitTracker* and evaluate its performance. The experiments show that the accuracy of rotation angles is around 3°, the accuracy of displacement is around 2.3%, and the accuracy of gait parameters is around 3%.

REFERENCES

[1] NaturalPoint. 2022. Optitrack. Retrieved on February 28, 2022 from https://optitrack.com/.
[2] Ziad O. Abu-Faraj, Gerald F. Harris, Peter A. Smith, and Sahar Hassani. 1999. Human gait and clinical movement analysis. In *Wiley Encyclopedia of Electrical and Electronics Engineering*. John Wily & Sons Inc. New York, 1–34.
[3] Boyd Anderson, Mingqian Shi, Vincent Y. F. Tan, and Ye Wang. 2019. Mobile gait analysis using foot-mounted UWB sensors. *Proc. ACM Interact. Mob. Wear. Ubiq. Technol.* 3, 3 (2019), 1–22.
[4] Terrell Bennett, Roozbeh Jafari, and Nicholas Gans. 2013. An extended kalman filter to estimate human gait parameters and walking distance. In *Proceedings of the American Control Conference*. IEEE, 752–757.
[5] James Diebel. 2006. Representing attitude: Euler angles, unit quaternions, and rotation vectors. *Matrix* 58, 15–16 (2006), 1–35.
[6] Moataz Eltoukhy, Jeonghoon Oh, Christopher Kuenze, and Joseph Signorile. 2017. Improved kinect-based spatiotemporal and kinematic treadmill gait assessment. *Gait Posture* 51 (2017), 77–83.
[7] Paul Gerdhem, Karin A. M. Ringsberg, Kristina Åkesson, and Karl J. Obrant. 2005. Clinical history and biologic age predicted falls better than objective functional tests. *J. Clin. Epidemiol.* 58, 3 (2005), 226–232.

[8] X. Gu, Fani Deligianni, Benny Lo, W. Chen, and Guang-Zhong Yang. 2018. Markerless gait analysis based on a single RGB camera. In *Proceedings of the IEEE 15th International Conference on Wearable and Implantable Body Sensor Networks (BSN'18)*. IEEE, 42–45.

[9] Jack M. Guralnik, Luigi Ferrucci, Eleanor M. Simonsick, Marcel E. Salive, and Robert B. Wallace. 1995. Lower-extremity function in persons over the age of 70 years as a predictor of subsequent disability. *New Engl. J. Med.* 332, 9 (1995), 556–562.

[10] Wenjun Jiang, Hongfei Xue, Chenglin Miao, Shiyang Wang, Sen Lin, Chong Tian, Srinivasan Murali, Haochen Hu, Zhi Sun, and Lu Su. 2020. Towards 3D human pose construction using Wifi. In *Proceedings of the 26th Annual International Conference on Mobile Computing and Networking (MobiCom'20)*. 1–14.

[11] Daniel J. Kuhman, Max R. Paquette, Shelby A. Peel, and Daniel A. Melcher. 2016. Comparison of ankle kinematics and ground reaction forces between prospectively injured and uninjured collegiate cross country runners. *Hum. Movement Sci.* 47 (2016), 9–15.

[12] S. O. H. Madgwick, A. J. L. Harrison, and R. Vaidyanathan. 2011. Estimation of IMU and MARG orientation using a gradient descent algorithm. In *Proceedings of the IEEE International Conference on Rehabilitation Robotics*. 1–7.

[13] Andrea Mannini and Angelo Maria Sabatini. 2014. Walking speed estimation using foot-mounted inertial sensors: Comparing machine learning and strap-down integration methods. *Med. Eng. Phys.* 36, 10 (2014), 1312–1321.

[14] Foued Melakessou. 2017. A New Sensor for Gait Analysis: Demonstration of the IEE's Smart Insole. In *Proceedings of the 15th ACM Conference on Embedded Network Sensor Systems*. ACM, 31.

[15] Zhen Meng, Song Fu, Jie Yan, Hongyuan Liang, Anfu Zhou, Shilin Zhu, Huadong Ma, Jianhua Liu, and Ning Yang. 2020. Gait recognition for co-existing multiple people using millimeter wave sensing. *Proceedings of the AAAI Conference on Artificial Intelligence* 34, 1 (2020), 849–856.

[16] Madhura Pathegama, Dileepa Marasinghe, Kanishka Wijayasekara, Ishan Karunanayake, Chamira Edussooriya, Pujitha Silva, and Ranga Rodrigo. 2018. Moving Kinect-Based Gait Analysis with Increased Range. In *Proceedings of the IEEE International Conference on Systems, Man, and Cybernetics (SMC'18)*. IEEE, 4126–4131.

[17] Tyagi Ramakrishnan, Seok Hun Kim, and Kyle B. Reed. 2019. Human gait analysis metric for gait retraining. *Appl. Bionics Biomech.* (2019).

[18] Julie D. Ries, John L. Echternach, Leah Nof, and Michelle Gagnon Blodgett. 2009. Test-retest reliability and minimal detectable change scores for the timed up and go test, the six-minute walk test, and gait speed in people with Alzheimer disease. *Phys. Therapy* 89, 6 (2009), 569–579.

[19] Anita Sant'Anna, Nicholas Wickström, Helene Eklund, Roland Zügner, and Roy Tranberg. 2012. Assessment of gait symmetry and gait normality using inertial sensors: in-lab and in-situ evaluation. In *Proceedings of the International Joint Conference on Biomedical Engineering Systems and Technologies*. Springer, 239–254.

[20] Sheng Shen, Mahanth Gowda, and Romit Roy Choudhury. 2018. Closing the gaps in inertial motion tracking. In *Proceedings of the 24th Annual International Conference on Mobile Computing and Networking*. ACM, 429–444.

[21] Sheng Shen, He Wang, and Romit Roy Choudhury. 2016. I am a smartwatch and i can track my user's arm. In *Proceedings of the 14th Annual International Conference on Mobile Systems, Applications, and Services*. 85–96.

[22] Chuyu Wang, Jian Liu, Yingying Chen, Lei Xie, Hong Bo Liu, and Sanclu Lu. 2018. RF-kinect: A wearable RFID-based approach towards 3D body movement tracking. *Proc. ACM Interact. Mob. Wear. Ubiq. Technol.* 2, 1 (2018), 1–28.

[23] Chen Wang, Jian Liu, Xiaonan Guo, Yan Wang, and Yingying Chen. 2019. WristSpy: Snooping passcodes in mobile payment using wrist-worn wearables. In *Proceedings of the IEEE Conference on Computer Communications (INFOCOM'19)*. IEEE, 2071–2079.

[24] Fei Wang, Sanping Zhou, Stanislav Panev, Jinsong Han, and Dong Huang. 2019. Person-in-WiFi: Fine-grained person perception using WiFi. In *Proceedings of the IEEE International Conference on Computer Vision*. 5452–5461.

[25] He Wang, Ted Tsung-Te Lai, and Romit Roy Choudhury. 2015. Mole: Motion leaks through smartwatch sensors. In *Proceedings of the 21st Annual International Conference on Mobile Computing and Networking*. 155–166.

[26] Wei Wang, Alex X. Liu, and Muhammad Shahzad. 2016. Gait recognition using wifi signals. In *Proceedings of the ACM International Joint Conference on Pervasive and Ubiquitous Computing*. 363–373.

[27] Wei Xu, ZhiWen Yu, Zhu Wang, Bin Guo, and Qi Han. 2019. AcousticID: Gait-based human identification using acoustic signal. *Proc. ACM Interact. Mob. Wear. Ubiq. Technol.* 3, 3 (2019), 1–25.

[28] Hongfei Xue, Yan Ju, Chenglin Miao, Yijiang Wang, Shiyang Wang, Aidong Zhang, and Lu Su. 2021. mmMesh: Towards 3D real-time dynamic human mesh construction using millimeter-wave. In *Proceedings of the 19th Annual International Conference on Mobile Systems, Applications, and Services*. 269–282.

[29] Yafeng Yin, Lei Xie, Tao Gu, Yijia Lu, and Sanglu Lu. 2019. AirContour: Building contour-based model for in-air writing gesture recognition. *ACM Trans. Sens. Netw.* 15, 4 (2019), 1–25.

[30] Hongyu Zhao, Zhelong Wang, Sen Qiu, Yanming Shen, and Jianjun Wang. 2017. IMU-based gait analysis for rehabilitation assessment of patients with gait disorders. In *Proceedings of the 4th International Conference on Systems and Informatics (ICSAI'17)*. IEEE, 622–626.

[31] Mingmin Zhao, Yonglong Tian, Hang Zhao, Mohammad Abu Alsheikh, Tianhong Li, Rumen Hristov, Zachary Kabelac, Dina Katabi, and Antonio Torralba. 2018. RF-based 3D skeletons. In *Proceedings of the Conference of the ACM Special Interest Group on Data Communication (SIGCOMM'18)*. 267–281.

[32] Daphne G. M. Zwartjes, Tjitske Heida, Jeroen P. P. Van Vugt, Jan A. G. Geelen, and Peter H. Veltink. 2010. Ambulatory monitoring of activities and motor symptoms in Parkinson's disease. *IEEE Trans. Biomed. Eng.* 57, 11 (2010), 2778–2786.

Received May 2021; revised November 2021; accepted November 2021